



Wind farm power optimization through wake steering

Michael F. Howland^a, Sanjiva K. Lele^{a,b}, and John O. Dabiri^{a,c,1}

^aDepartment of Mechanical Engineering, Stanford University, Stanford, CA 94305; ^bDepartment of Astronautics and Aeronautics, Stanford University, Stanford, CA 94305; and ^cDepartment of Civil and Environmental Engineering, Stanford University, Stanford, CA 94305

Edited by Alexis T. Bell, University of California, Berkeley, CA, and approved May 20, 2019 (received for review March 4, 2019)

Global power production increasingly relies on wind farms to supply low-carbon energy. The recent Intergovernmental Panel on Climate Change (IPCC) Special Report predicted that renewable energy production must leap from 20% of the global energy mix in 2018 to 67% by 2050 to keep global temperatures from rising 1.5 °C above preindustrial levels. This increase requires reliable, low-cost energy production. However, wind turbines are often placed in close proximity within wind farms due to land and transmission line constraints, which results in wind farm efficiency degradation of up to 40% for wind directions aligned with columns of turbines. To increase wind farm power production, we developed a wake steering control scheme. This approach maximizes the power of a wind farm through yaw misalignment that deflects wakes away from downstream turbines. Optimization was performed with site-specific analytic gradient ascent relying on historical operational data. The protocol was tested in an operational wind farm in Alberta, Canada, resulting in statistically significant ($P < 0.05$) power increases of 7–13% for wind speeds near the site average and wind directions which occur during less than 10% of nocturnal operation and 28–47% for low wind speeds in the same wind directions. Wake steering also decreased the variability in the power production of the wind farm by up to 72%. Although the resulting gains in annual energy production were insignificant at this farm, these statistically significant wake steering results demonstrate the potential to increase the efficiency and predictability of power production through the reduction of wake losses.

wind energy | turbulence | data science

The Intergovernmental Panel on Climate Change (IPCC) Special Report 15 on global warming (1) found that current rates of emissions will result in a temperature rise from preindustrial levels of 1.5 °C by 2040. Meanwhile, recent studies have predicted that the Paris Climate Agreement (2) will fail to keep warming below the stated goal of 2 °C (3, 4). The Special Report 15 found that coal-based electricity generation must decrease from contemporary rates of 40% of global energy production to 1–7%. As a result, renewable energy should compensate for this transition, increasing from 20% of energy generation in 2018 to 67% by 2050 (1). Wind and solar will likely comprise the bulk of these capacity additions due to their decreasing cost of electricity (5). While recent studies (5) have shown onshore wind energy to be economically favorable compared with coal and combined-cycle natural gas, such estimates are specific to sites with robust, reliable wind resource. To reach the goals of the Paris Climate Agreement, wind farms must significantly increase in number and density as well as extend to sites with less certain wind resource (6). As a result, methods to increase wind farm efficiency remain paramount to reducing carbon emissions.

While the major reason for decreased wind farm efficiency is variability in wind speed, aerodynamic losses within large arrays of turbines are also a key issue in wind farm operation (7). Due to the process of energy extraction from the atmospheric boundary layer, wind turbines necessarily produce a reduced momentum wake region immediately downstream (8). This wake will lower the power production of downstream turbines in the array. Wake power losses within a wind farm are a function of the incident wind speed and direction.

Wake losses occur when the wind speed is below the rated value (9) and turbines are at least partially aligned to the angle of the incoming wind. The mean wind speeds at the majority of wind farms are well below the rated value (10). Wind directions in the turbulent atmospheric boundary layer are inherently variable and will vary with the time of day, season, and other geophysical parameters (11). Wind farm layouts are designed to extract the maximum profit given historically observed wind direction and speed distributions, which typically results in larger streamwise turbine spacing in the most common wind directions. However, for other wind directions, wind turbines are more closely spaced (12). In worst-case scenarios of wind turbine spacing and inflow directions in contemporary wind farms, there is an over 40% loss of efficiency when the wind shifts to a direction aligned with the columns of the turbines (13).

To minimize the aerodynamic losses between turbines under prevailing wind conditions, the optimal streamwise spacing has been found to be 10–15 D , where D is the turbine diameter (14–16). Modern turbines are increasing in size, with offshore turbines now above 200 m in rotor diameter (17). The corresponding spacing of turbines multiple kilometers apart significantly increases the cost of transmission lines and land use (18). As a result, wind farm designers are left with a complex multiobjective optimization problem which typically results in operational turbine spacing of 6–10 D (18). At this spacing, significant aerodynamic wake losses persist in modern wind farms when the flow is aligned with columns of turbines and the wind speed is below the rated value (13).

While the influence of wake losses on wind farm efficiency can be large for some inflow directions, the cumulative impact on the annual energy production of smaller wind farms is generally

Significance

Wake effects within wind farms can significantly decrease the power production and increase the cost of electricity. Herein, we designed a wake steering control scheme to increase the power production of wind farms. The wake steering method was tested in an array of six utility-scale turbines where it increased the power production for wind speeds near the site annual average between 7% and 13% and decreased variability by up to 72%, for selected wind directions at night. These improvements can contribute to the increasing ability of wind farms to provide reliable, low-cost, and efficient base energy load.

Author contributions: M.F.H. and J.O.D. designed research; M.F.H. performed research; M.F.H., S.K.L., and J.O.D. contributed new analytic tools; M.F.H., S.K.L., and J.O.D. analyzed data; and M.F.H., S.K.L., and J.O.D. wrote the paper.

The authors declare no conflict of interest.

This article is a PNAS Direct Submission.

This open access article is distributed under Creative Commons Attribution-NonCommercial-NoDerivatives License 4.0 (CC BY-NC-ND).

Data deposition: The data from this paper have been deposited in the Stanford Digital Repository, <https://purl.stanford.edu/rn821pp7681>.

¹To whom correspondence may be addressed. Email: jodabiri@stanford.edu.

This article contains supporting information online at www.pnas.org/lookup/suppl/doi:10.1073/pnas.1903680116/-DCSupplemental.

lower since turbines are well spaced in directions of high wind speed. However, the impact of wake losses can be significant, as in the Horns Rev offshore wind farm where they have been found to reduce annual energy production on the order of 20% (13, 19). With wind farms increasing in size and quantity (20), wake losses are becoming an increasingly important factor in wind farm efficiency (21). While the magnitude of wake-induced efficiency degradation will depend on the specific wind farm site, methods which can reduce wake losses, once developed, will likely be broadly applicable to the global wind energy fleet. As such, potential wake mitigation methods have been a focus for multiyear research initiatives operated by the US Department of Energy such as the Atmosphere to Electrons (A2e) campaign and the Scaled Wind Farm Technology (SWiFT) facility (22). Given the broad potential impact of a method to mitigate wake losses, we have developed a control scheme and tested it on six utility-scale turbines in a wind farm in Alberta, Canada for wind speeds and directions where wake losses have been observed historically. Our method increased the power production for these wind directions between 7% and 13% for moderate wind speeds near the site annual average and up to 47% for low wind speeds, representing a statistically significant demonstration of wake steering power optimization for a multiturbine wind farm.

Aside from mean power production, wind turbine wakes contribute to intermittency. Intermittent power production is caused both by wind fluctuations in the turbulent atmospheric boundary layer and by the inherent nonlinearity of wind turbine power generation as a function of wind speed (23). Further, turbine wakes contribute to the lack of precise controllability of the wind farm power production. Intermittent renewable energy resources increase the need for costly energy reserve systems to guarantee grid service reliability (24). When wind speeds are low, wind turbines may oscillate about the cut-in speed as a result of wind gusts and dynamic wake meandering (25). Control methods which reduce the variability of the power production of wind farms, measured here as the SD of the time record of power generation, can decrease the ancillary service requirements for the energy grid (26). Our method, applied at the wind farm in Alberta, Canada, reduced the SD of the wind farm power production up to 72% for the wind conditions of interest.

Wake Steering Control

Recent attention has focused on mitigation of wake losses through the use of turbine control protocols and systems optimization that sacrifices individual turbine performance to improve the collective wind farm performance. Several studies have attempted to optimize the power generation of a wind farm through the operation of the upstream turbine in a suboptimal state to increase the efficiency of a downstream turbine (27, 28), but the results have not yet provided a conclusive solution that can be extrapolated to arbitrary wind farm configurations (29).

Contemporary turbine operation minimizes the yaw misalignment angle, which is the angle between the axis of the turbine nacelle and the incoming wind direction. While wind turbines typically exhibit small yaw misalignment due to control errors and sensor noise and uncertainty (30), the goal of industrial control algorithms is to minimize this yaw. When misaligned with respect to the incoming wind, wind turbines impose a lateral forcing which deflects the wake region (31), as sketched in Fig. 1A. While the misaligned turbine generates suboptimal power, the wake may no longer directly impinge upon a downstream turbine as a result of the wake steering. An application of wake steering for a six-turbine wind farm is shown in Fig. 1B and C. Such a control strategy has been shown to be beneficial for downwind turbines in a number of wind tunnel experiments (32, 33) and computational studies (34–37). Wake

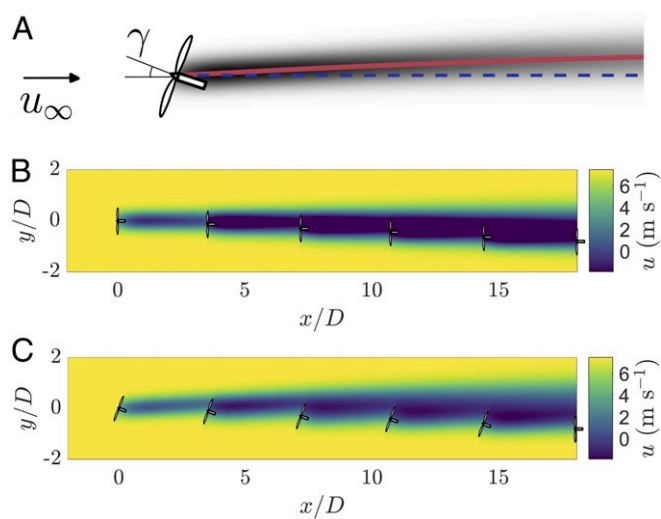


Fig. 1. (A) A wind turbine with diameter D yawed at angle γ with respect to the incoming wind and viewed from above. The incoming wind at speed u_∞ is incident from the left. The centerline of an unyawed, standard operational wake would follow the dashed blue line. The centerline of the yawed wake follows the solid red line. (B and C) Wake model streamwise velocity field for baseline maximum power point tracking control (B) and optimal yaw control (C). The incoming wind speed at the most upstream turbine is $u_\infty = 7.5 \text{ m}\cdot\text{s}^{-1}$ and there are six turbines modeled. The wake following turbine six is not shown since the wake model automatically neglects calibration of the parameters for turbine six to increase computational efficiency.

steering has also been used in a two-turbine field experiment which demonstrated an increase in the downwind turbine power production as a function of the atmospheric stability (38). The impact of wake steering on the sum of the upwind and downwind turbines' power production was inconclusive in a separate two-turbine field experiment (39). Here we demonstrate a statistically significant effect of wake steering in a field study with a six-turbine unit.

Due to experimental difficulty and computational expense, parametric studies and real-time wind farm power optimization are limited with previous approaches (29). As such, the development of an accurate and computationally efficient model for wind farm power generation as a function of wake steering actuation is required to facilitate real-time closed-loop control (40).

Site-Specific Power Optimization

The wind turbine power, P , is a function of the wind farm layout and inflow conditions. Additionally, a wind turbine's power production is a function of its yaw misalignment angle as well as the yaw misalignment of upstream turbines which manifests as wake deflections. We have developed an analytic formulation to predict wind turbine power production as a function of atmospheric conditions and the yaw misalignment decisions of upwind turbines. Wake steering is captured using a recently developed lifting line model (41). While the magnitude of wake steering (42) and the wind speed and direction (43) are functions of the vertical dimension, the measurements available at the site in the present study were limited to point-wise sensors at hub height. While the incorporation of the curled-wake three dimensionality (42) may improve the model accuracy in certain atmospheric conditions, a 2D model is sufficient to capture the key physics for the present wind farm experiment. Details of the analytic predictive wake model are given in *SI Appendix*. The maximization of the wind farm power production through the use of wake steering is posed as an optimization,

$$\begin{aligned} & \underset{\vec{\gamma}}{\text{maximize}} && \sum_{i=1}^{N_t} P_i \\ & \text{subject to} && \gamma_i \in [\gamma_{\min}, \gamma_{\max}], \end{aligned} \quad [1]$$

where γ_i is the yaw angle for turbine i , N_t is the number of turbines, and γ_{\min} and γ_{\max} are bounds on the yaw misalignment for each turbine. Eq. 1 is not convex but can be optimized using a number of algorithms. Similar studies have previously used genetic algorithms (44) or discrete gradients (35). Since we have developed an analytic function to predict wind farm power production, Eq. 1 can be optimized efficiently using analytic gradients combined with the common gradient ascent strategy called Adam optimization (45).

Site-Specific Wake Model Calibration

The model (*SI Appendix*) is calibrated using utility-scale field historical data from five 1.8-MW Vestas V80 wind turbines and one 2.0-MW Vestas V80 turbine at an operational wind farm in Alberta, Canada. The six turbines in the wind farm are aligned at $\sim 335^\circ$, where north is 0° and the angle proceeds clockwise to 360° at north again. With wind inflow from 335° , the turbines are spaced by $\sim 3.5D$ in the prevailing wind direction. The wind inflow conditions are prescribed by the supervisory control and data acquisition (SCADA) nacelle-mounted measurements of wind speed and nacelle direction. Turbulence intensities were not measured in the present study due to the wind turbine hardware limitations. Details of the wind condition measurements are discussed in *SI Appendix*. Five years of 1-min averaged SCADA operational data, including power, nacelle direction, and wind speed, were used to calibrate the proportionality constant of the presumed Gaussian wake and the wake spreading coefficient. The latter parameter dictates the wake diameter which is a function of the streamwise distance following a wind turbine. This model allows each turbine to have independent values for the two model parameters, since these parameters are known to be a function of the atmospheric boundary layer conditions (46) as well as the number of upwind turbines (47). The model parameters were determined using analytic gradient descent (*SI Appendix*). The resulting calibrated model using the nocturnal historical baseline data is shown in Fig. 2 for $330^\circ \pm 5^\circ$ inflow at $u_\infty = 5\text{--}6\text{ m}\cdot\text{s}^{-1}$ and $u_\infty = 7\text{--}8\text{ m}\cdot\text{s}^{-1}$. The power productions are normalized by the power of the most upwind turbine. The second turbine, on average, produces $\sim 30\%$ and 40% of the upstream turbine's power in the low and moderate wind speed cases, respectively. Wake losses are larger for lower wind speeds due to the higher relative thrust that the turbine imparts upon the velocity field at low wind speeds.

The model fit for the moderate wind speed has mean absolute error of 0.02 while the low wind speed fit has mean absolute error of 0.09 (given as a ratio normalized by the power of the first tur-

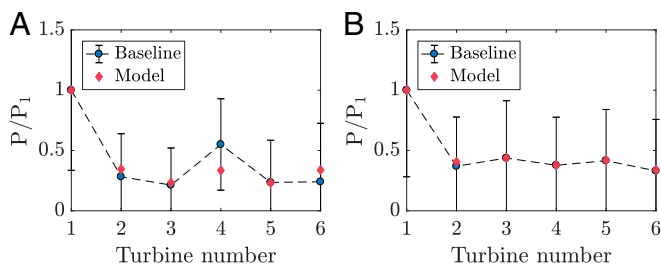


Fig. 2. (A and B) Wake model calibration using 5 y of historical SCADA turbine power data for inflow from $330^\circ \pm 5^\circ$ for (A) $u_\infty = 5\text{--}6\text{ m}\cdot\text{s}^{-1}$ and (B) $u_\infty = 7\text{--}8\text{ m}\cdot\text{s}^{-1}$. Error bars represent 1 SD in the data. Turbine 4 is a Vestas V80 2.0-MW machine while the rest are Vestas V80 1.8 MW. The turbine power productions are normalized by the most upwind turbine P_1 .

bine). The less accurate fit in the low wind speed bin is expected due to the inherent nonlinearity at the effective cut-in velocity of $5\text{ m}\cdot\text{s}^{-1}$ for the Vestas V80 turbines at the site of interest. Specifically, above cut-in, the turbine generates power and imparts drag on the fluid, creating a wake region. Below the cut-in, zero power is produced and no significant wake region exists. Due to dynamic wake meandering, downstream turbines will fluctuate between cut-in and shutdown for very low wind speeds and static models that consider only time-averaged behavior are not able to capture these dynamics as well (48). This is illustrated in Fig. 2A where zero power production occurs within 1 SD of the mean. Since the yaw controller on the Vestas V80 turbines did not allow for dynamic yaw maneuvers, such dynamic extensions were not applicable in the modeling framework. Wake model calibrations for other northwest wind inflow directions and speeds are not shown for brevity.

Field Experiment Design

While the wind farm in Alberta was designed for high-speed flow from the southwest, nocturnal low to moderate wind speeds from the northwest occur during the summer and fall. The present experiment aimed to optimize the yaw misalignment angles for these wind speeds from the northwest for which there are significant wake effects.

The yaw misalignment optimization was run with the calibrated model for inflow from 315° to 355° for which wake losses are observed. These angles represent $\sim 8\%$ of the nocturnal operation of the wind farm with nearly all of the samples occurring in the summer and fall seasons. The historical data wind rose is shown in *SI Appendix*, Fig. S1A. The yaw angle optimization resulted in $\sim 20^\circ$ clockwise yaw misalignment with respect to the incoming wind for each of the first five turbines in the column and zero misalignment for the turbine that was farthest downwind. Due to the hardware limitations of the yaw control systems of the wind turbines, only one set of yaw misalignment angles could be chosen for the range of northwest inflow. Therefore, the misaligned turbines were persistently offset by 20° for all northwest inflow directions, from 315° to 355° . While turbulence intensity measurements were not available at the wind farm site, the nocturnal operation typically results in fairly low turbulence intensity and therefore larger wake losses due to suppressed mixing in the wakes (11). Details of the yaw misalignment optimization are given in *SI Appendix*. Other yaw misalignment angles were not tested due to experimental limitations of implementation and to increase the number of unique days of experimentation with one set of misalignments. The longer experiment duration was necessary to achieve statistical confidence.

The present control-based optimization strategy was tested in a full-scale field experiment of the six utility-scale turbines from October 15 until October 25 of 2018. A photo of the yaw-misaligned turbines can be seen in Fig. 3A. A top-view sketch of the optimal yaw angles for reference inflow from the northwest can be seen in Fig. 3B.

Field Experiment Results

Significant power increases over the baseline were observed for low to moderate wind speeds from the northwest. The impact of the wake steering on the mean and SD of the power production for the northwest inflow conditions is shown in Table 1. Wind directions and speeds with more than 15 1-min-averaged data samples are shown.

For low wind speeds of $u_\infty = 5\text{--}6\text{ m}\cdot\text{s}^{-1}$ and $325^\circ \pm 5^\circ$ inflow, the total power of the six turbines increased from a temporal average of 390 kW to 570 kW, representing a 47% increase. Meanwhile, for $330^\circ \pm 5^\circ$ inflow at $u_\infty = 5\text{--}6\text{ m}\cdot\text{s}^{-1}$, the power increase was 28% (Fig. 3C). The large percent increases in these cases are due to the low power production at low wind speeds and the proximity of the wind speeds to the cut-in speed of $5\text{ m}\cdot\text{s}^{-1}$.

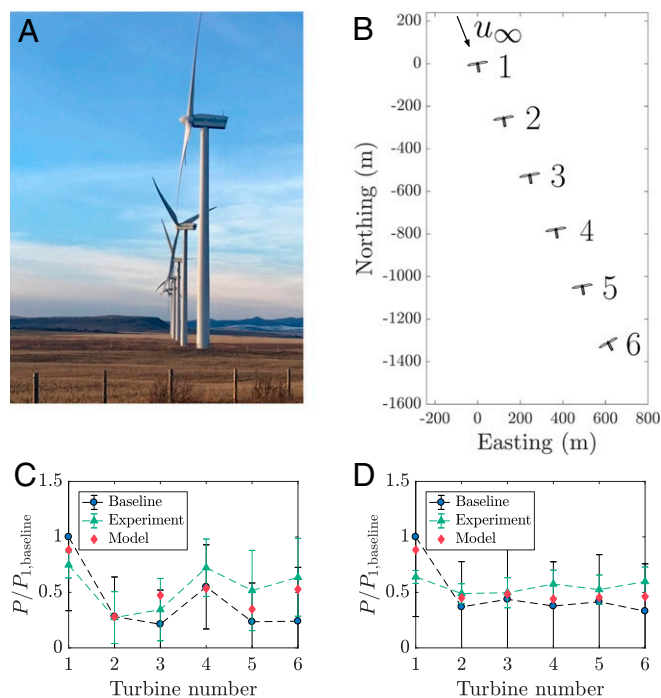


Fig. 3. (A) Photo of the six Vestas V80 turbines at the operational wind farm in Alberta, Canada. (B) Top view of the optimized yaw misalignment for the six turbines. The flow originates from the northwest, the inflow condition of interest for the present optimization experiment. Turbines one through five are misaligned 20° clockwise with respect to the incoming wind. Turbine six is not misaligned. Coordinates are in meters. (C and D) The power as a function of turbine number is compared for baseline operation with 5 y of historical SCADA data (blue circles), the experimental yaw campaign (green triangles), and the model predictions (red diamonds) based on the calibrations given in Fig. 2. The inflow conditions are shown for $330^\circ \pm 5^\circ$ at (C) $u_\infty = 5\text{--}6\text{ m}\cdot\text{s}^{-1}$ and (D) $u_\infty = 7\text{--}8\text{ m}\cdot\text{s}^{-1}$. Error bars represent 1 SD in the data.

The significant improvement in these two cases can be attributed to the deflection of the upstream wakes. Partial wake overlap occurs when a section of the wind turbine rotor area is in the wake of an upwind turbine while another section is in unperturbed, freestream flow. Such a case occurs for the six turbines with flow from 325° to 330° . During the partial wake scenario, a small yaw misalignment for the upwind turbine can result in the downstream turbine operating exclusively in freestream conditions. The reduction in the occurrence of partial wakening is beneficial for power generation and significantly reduces turbine fatigue and failure (49). The model captures the influence of yaw misalignment in the partial wake scenario as shown in Fig. 1 B and C, where the wakes of the upstream turbines are deflected

away from downstream turbines. The wakes impact the downstream turbines more directly at 330° than at 325° . As a result, larger wake deflections are required at 330° than at 325° to steer the wake away from the downstream turbines. Therefore, the anticipated power increase is higher for 325° where the partial wake scenario is most prominent.

For the higher wind speed of $u_\infty = 7\text{--}8\text{ m}\cdot\text{s}^{-1}$ from $330^\circ \pm 5^\circ$ the total power increased from 1.86 MW to 2.11 MW, a 13% increase (Fig. 3D). The percentage increase is less in the higher wind speed cases as a result of the decreased wake effects at these speeds.

Flow directly impinging along the alignment of the wind farm column at $335^\circ \pm 5^\circ$ occurred significantly only at wind speeds between $u_\infty = 7\text{--}8\text{ m}\cdot\text{s}^{-1}$. For these conditions, the power production of the six turbines increased by 7%. Wind farms are typically sited at locations in which the mean wind speed is around $8\text{ m}\cdot\text{s}^{-1}$ (10). Therefore, for wind farms with similar streamwise spacing and direct alignment, the 7% power increase observed in this wind condition is expected on average.

Wake steering also significantly reduced the variability in the sum of the six-turbine power production, measured here as a SD in the time series of 1-min-averaged data (Table 1). The reduction in the SDs of the sum of power is due to the diminished wake effects between the turbines. This manifests as a notable decrease in the percentage of time the turbines are not producing power (off rate) for all wind conditions. It is worth noting that all of the wind conditions considered here are above the cut-in speed of the Vestas V80 turbines and therefore without wake effects the off rate would be 0% for all wind condition cases. The high off rates in the baseline control case result from the impinging speed to a given turbine dropping below the cut-in speed. As a result of the wake steering, the percentage of time in which the speed decreases below the cut-in value for the downwind turbines has appreciably dropped.

The low-order model is able to predict the effect of the yawing action on the trends of power production in the field experiment based on calibration using only historical data (Fig. 3 C and D). As expected, the power production of turbine one (i.e., the most upwind turbine) was reduced due to operation with yaw misalignment. However, the power production of turbines two through five, and especially the farthest downwind turbine six, increased significantly. There are discrepancies in the low wind speed case shown in Fig. 3C as a result of the cut-in speed nonlinearity and dynamic wake meandering not captured in the model. However, the qualitative agreement with the model prediction trends promotes the use of the present model for real-time control of arbitrary, utility-scale wind farms.

The largest source of error in the present modeling framework is the functional dependence of power on the yaw misalignment angle. In the present approach, the power production as a function of yaw was assumed to follow the wind tunnel experimental result of $\cos^2(\gamma)$ (50). While this model works fairly

Table 1. Six utility-scale wind turbine wake steering effects on the mean (Δ_m), SD(Δ_s), and off rate of power production compared with the baseline operation

Wind inflow: Direction, $^\circ$	Wind inflow: Speed, $\text{m}\cdot\text{s}^{-1}$	Experimental results				No. of data points
		Δ_m , %	Δ_s , %	Baseline off rate, %	Yawed off rate, %	
320	5–6	–13	–53	31	24	65
325	5–6	+47	–20	36	13	52
325	6–7	+24	+2	24	12	25
330	5–6	+28	–14	27	10	17
330	7–8	+13	–72	18	0	22
335	7–8	+7	–73	12	0	22

Conditions of northwest inflow with more than 15 1-min-averaged samples are shown.

Table 2. Two-sample Kolmogorov–Smirnov statistical test for the null hypothesis that the baseline historical SCADA power data and the experimental yaw misalignment power data are samples of the same distribution

Wind inflow: Direction, °	Wind inflow: Speed, m·s ⁻¹	<i>P</i> values		
		Full	10,000	100,000
320	5–6	0.13	0.14	0.14
325	5–6	$2.3 \cdot 10^{-7}$	$6.1 \cdot 10^{-4}$	$6.1 \cdot 10^{-4}$
325	6–7	0.043	0.32	0.32
330	5–6	0.039	0.27	0.27
330	7–8	$6.9 \cdot 10^{-6}$	0.015	0.015
335	7–8	$8.0 \cdot 10^{-5}$	0.03	0.03

The Kolmogorov–Smirnov test is run with the full historical dataset (full) and with Monte Carlo sampling from the full dataset such that the number of samples is consistent between the baseline and the experimental campaign. The Monte Carlo statistical method is run for 10,000 and 100,000 random samples to demonstrate convergence.

well in the low wind speed case shown in Fig. 3C, it is inaccurate for the higher wind speed case shown in Fig. 3D. As a result, there is likely a functional dependency of the exponent of cosine on the incoming wind speed as well as the previously reported dependence on the turbine type (44) and shear and veer in the atmospheric boundary layer.

The power increase results are statistically significant ($P < 0.05$) according to a two-sample Kolmogorov–Smirnov test. The details of the statistical experiments are shown in *Materials and Methods*. However, the statistical test does not examine the dominant causes of uncertainty, which are atmospheric boundary layer inflow conditions including wind speed and direction and the limited number of unique days of the experimental yaw campaign. The full dataset can be accessed at <https://purl.stanford.edu/rn821pp7681>.

Discussion

We demonstrate a statistically significant utility-scale field experiment of wake steering increasing the power production of a multiturbine wind farm for wind conditions which exhibit wake losses. While the impact of wake steering on annual energy production is site specific (e.g., below 0.3% at this wind farm), this experiment serves as a proof of concept for the potential of wake steering to significantly mitigate wake losses which reduce the annual energy production of wind farms (13). Wake steering control also decreased power production intermittency. Since frequency regulation ancillary services are required on the timescale of minutes (26), the SDs with respect to 1-min-averaged time series of power production are relevant to energy grid planning. This demonstrates that wake steering has the potential to reduce the intermittency of wind energy and thus improve the reliability of this component of the energy grid. Advances in our understanding of the physics of wind farms, combined with improvements in modeling, design, and control optimization, will further expand the value of this renewable energy technology and its ability to provide low-cost and reliable energy for a sustainable grid.

Achieving these potential power increases in the global wind farm fleet requires an efficient computational model. The present analytic model formulation was chosen due to its computational efficiency, which facilitates its use for real-time control of utility-scale wind farms. The computational cost of previous methods scales as $O(N_x N_y)$, where N_x and N_y are the number of grid points used in the computational domain, whereas the cost of the present method scales as $O(N_t)$, where N_t is the number of turbines. Typically, $O(10)$ grid points are used for each turbine in the wind farm (34), leading to an approximate scaling of $O(100N_t^2)$. Therefore, the present method has a computa-

tional reduction of at least two orders of magnitude. This scaling enables real-time model calibration and wind farm control using only a standard personal computer. Given that all utility-scale wind turbines are constructed with yaw controllers, the present control scheme can be directly implemented into any operational wind farm, thus immediately increasing the energy outputs from these sites with no additional cost.

Recent simulations have noted a potential influence of the direction of yaw misalignment on the power production in a simplified, aligned, two-wind-turbine wake steering scenario (51, 52). This observation has not been corroborated in all other wake steering studies and is likely a strong function of the turbine layout (53). The potential asymmetry in the power production as a function of the direction of yaw misalignment is likely caused by the curled, 3D wake (42) and the wind velocity veer and shear. Recent work suggests that this asymmetry is due to the Coriolis effect (37). These effects are the subject of ongoing modeling work (36, 43, 54, 55) and were therefore not included in the present framework.

Aside from the effect of yaw misalignment on power production observed here, wake steering will also have an impact on wind turbine unsteady loading and therefore mechanical fatigue. Theoretical and numerical studies have predicted that yaw misalignment can reduce or increase the mechanical fatigue loading on wind turbine blades, depending on the direction of yaw misalignment (56). However, the influence of yaw misalignment on fatigue loading is a function of the specific wind turbine and control system as recent studies have reported differing results, depending on the wind turbine of interest (49, 57). Further, yaw misalignment can reduce the occurrence of partial wake overlap which is known to significantly increase fatigue loading (58). In the experiment described here at a wind farm in Alberta, partial wake overlap decreased significantly. While the wind turbine fatigue loading was not measured in the present field experiment, it is the subject of future work and instrumentation at this field site. More generally, accurate predictions of the influence of yaw misalignment on the fatigue loading of all of the wind turbines in the wind farm will likely be required before the broad implementation of wake steering as the optimal control scheme for utility-scale wind farms. This is the subject of ongoing work through the Department of Energy A2e program through the use of the National Renewable Energy Laboratory's FAST simulation tool (59).

Materials and Methods

Statistical Tests. The statistical significance of the experimental yaw power optimization results was tested using the two-sample Kolmogorov–Smirnov test. The Kolmogorov–Smirnov test was selected since the datasets are non-normal distributions. The null hypothesis is that the sum of the six-turbine power generations from the baseline historical data and the experimental yaw measurements are the same distributions. The statistical test is run for the specific inflow conditions shown in Table 1. There are more than an order of magnitude more samples from the historical baseline dataset than for the yaw campaign due to the limited length of the field experiment. As such, the *P* values are computed using random sampling from the full distribution such that the baseline dataset has the same number of data points as the yaw misalignment experiment data. The *P* values are then averaged together as a Monte Carlo method. The resulting *P* values are shown in Table 2. All results are statistically significant ($P < 0.05$) except for inflow from $320^\circ \pm 5^\circ$ at a speed of $5\text{--}6\text{ m}\cdot\text{s}^{-1}$. The samples during the experimental yaw misalignment campaign are not strictly independent since they may occur during similar atmospheric boundary layer conditions. The results are similar if smaller wind speed or direction bins are used to calculate conditional averages. The full dataset can be accessed at <https://purl.stanford.edu/rn821pp7681>.

ACKNOWLEDGMENTS. We thank TransAlta Corporation and TransAlta Renewables for graciously providing historical wind farm operational data and for performing the yaw misalignment experimental campaign on operational turbines. M.F.H. is funded through a National Science Foundation Graduate Research Fellowship under Grant DGE-1656518 and a Stanford Graduate Fellowship.

1. Intergovernmental Panel on Climate Change. "Summary for policymakers" in *Global Warming of 1.5°C. An IPCC Special Report on the Impacts of Global Warming of 1.5°C Above Pre-Industrial Levels and Related Global Greenhouse Gas Emission Pathways, in the Context of Strengthening the Global Response to the Threat of Climate Change, Sustainable Development, and Efforts to Eradicate Poverty*, V. Masson-Delmotte et al., Eds. (World Meteorological Organization, Geneva, Switzerland, 2018).
2. UNFCCC, "Adoption of the Paris agreement" (Report No. FCCC/CP/2015/L.9/Rev.1, 2015).
3. J. Rogelj et al., Paris agreement climate proposals need a boost to keep warming well below 2 C. *Nature* **534**, 631–639 (2016).
4. K. Anderson, G. Peters, The trouble with negative emissions. *Science* **354**, 182–183 (2016).
5. EIA, "Annual Energy Outlook" (AEO2018, 2018).
6. C. L. Archer, M. Z. Jacobson, Evaluation of global wind power. *J. Geophys. Res. Atmos.* **110**, 110.D12 (2005).
7. R. Wiser, M. Bolinger, "2017 wind technologies market report" (Tech. Rep. DOE/EE-1798, US Department of Energy Office of Energy Efficiency and Renewable Energy, US Department of Energy Office of Scientific and Technical Information, Oak Ridge, TN, 2017).
8. L. Vermeer, J. N. Sørensen, A. Crespo, Wind turbine wake aerodynamics. *Prog. Aerospace Sci.* **39**, 467–510 (2003).
9. M. A. Abdullah, A. Yatim, C. W. Tan, R. Saidur, A review of maximum power point tracking algorithms for wind energy systems. *Renewable Sustainable Energy Rev.* **16**, 3220–3227 (2012).
10. C. Draxl, A. Clifton, B. M. Hodge, J. McCaa, The wind integration national dataset (wind) toolkit. *Appl. Energy* **151**, 355–366 (2015).
11. K. S. Hansen, R. J. Barthelmie, L. E. Jensen, A. Sommer, The impact of turbulence intensity and atmospheric stability on power deficits due to wind turbine wakes at Horns Rev wind farm. *Wind Energy* **15**, 183–196 (2012).
12. R. J. Stevens, C. Meneveau, Flow structure and turbulence in wind farms. *Annu. Rev. Fluid Mech.* **49**, 311–339 (2017).
13. R. J. Barthelmie et al., Modelling and measuring flow and wind turbine wakes in large wind farms offshore. *Wind Energy* **12**, 431–444 (2009).
14. G. Marmidis, S. Lazarou, E. Pyrgioti, Optimal placement of wind turbines in a wind park using Monte Carlo simulation. *Renewable Energy* **33**, 1455–1460 (2008).
15. J. Meyers, C. Meneveau, Optimal turbine spacing in fully developed wind farm boundary layers. *Wind Energy* **15**, 305–317 (2012).
16. R. J. Stevens, D. F. Gayme, C. Meneveau, Effects of turbine spacing on the power output of extended wind-farms. *Wind Energy* **19**, 359–370 (2016).
17. General Electric, "GE announces Haliade-X, the world's most powerful offshore wind turbine" (2018). <https://www.ge.com/renewableenergy/wind-energy/offshore-wind/haliade-x-offshore-turbine>. Accessed 15 December 2018.
18. R. J. Stevens, B. F. Hobbs, A. Ramos, C. Meneveau, Combining economic and fluid dynamic models to determine the optimal spacing in very large wind farms. *Wind Energy* **20**, 465–477 (2017).
19. M. Gaumond et al., "Benchmarking of wind turbine wake models in large offshore windfarms" in *The Science of Making Torque from Wind 2012: 4th Scientific Conference*, E. Seidel, D. Heinemann, M. Kühn, J. Peinke, S. Barth (IOP Publishing, Bristol, UK, 2012), vol. 555.
20. M. Z. Jacobson, M. A. Delucchi, A path to sustainable energy by 2030. *Sci. Am.* **301**, 58–65 (2009).
21. J. Lundquist, K. DuVivier, D. Kaffine, J. Tomaszewski, Costs and consequences of wind turbine wake effects arising from uncoordinated wind energy development. *Nat. Energy* **4**, 26–34 (2019).
22. J. Berg et al., "Scaled wind farm technology facility overview" in *32nd ASME Wind Energy Symposium* (ASME, New York, NY, 2014), p. 1088.
23. P. Milan, M. Wächter, J. Peinke, Turbulent character of wind energy. *Phys. Rev. Lett.* **110**, 138701 (2013).
24. T. Das, V. Krishnan, J. D. McCalley, Assessing the benefits and economics of bulk energy storage technologies in the power grid. *Appl. Energy* **139**, 104–118 (2015).
25. G. C. Larsen, H. A. Madsen, K. Thomsen, T. J. Larsen, Wake meandering: A pragmatic approach. *Wind Energy* **11**, 377–395 (2008).
26. D. Nock, V. Krishnan, J. D. McCalley, Dispatching intermittent wind resources for ancillary services via wind control and its impact on power system economics. *Renewable Energy* **71**, 396–400 (2014).
27. J. R. Marden, S. D. Ruben, L. Y. Pao, A model-free approach to wind farm control using game theoretic methods. *IEEE Trans. Control Syst. Technol.* **21**, 1207–1214 (2013).
28. J. Annoni, P. M. Gebraad, A. K. Scholbrock, P. A. Fleming, J. W. v. Wingerden, Analysis of axial-induction-based wind plant control using an engineering and a high-order wind plant model. *Wind Energy* **19**, 1135–1150 (2016).
29. S. Boersma et al., "A tutorial on control-oriented modeling and control of wind farms" in *2017 American Control Conference (ACC)* (IEEE, Piscataway, NJ, 2017), pp. 1–18.
30. P. Fleming et al., Field-test results using a nacelle-mounted lidar for improving wind turbine power capture by reducing yaw misalignment. *J. Phys. Conf. Ser.* **524**, 012002 (2014).
31. Á. Jiménez, A. Crespo, E. Migoya, Application of a LES technique to characterize the wake deflection of a wind turbine in yaw. *Wind Energy* **13**, 559–572 (2010).
32. M. Adaramola, P. Å. Krogstad, Experimental investigation of wake effects on wind turbine performance. *Renewable Energy* **36**, 2078–2086 (2011).
33. F. Mühle et al., Blind test comparison on the wake behind a yawed wind turbine. *Wind Energy Sci.* **3**, 2, 883–903 (2018).
34. P. A. Fleming, A. Ning, P. M. Gebraad, K. Dykes, Wind plant system engineering through optimization of layout and yaw control. *Wind Energy* **19**, 329–344 (2016).
35. P. Gebraad, J. J. Thomas, A. Ning, P. Fleming, K. Dykes, Maximization of the annual energy production of wind power plants by optimization of layout and yaw-based wake control. *Wind Energy* **20**, 97–107 (2017).
36. P. Fleming et al., A simulation study demonstrating the importance of large-scale trailing vortices in wake steering. *Wind Energy Sci.* **3**, 243–255 (2018).
37. C. L. Archer, A. Vassel-Behag, Wake steering via yaw control in multi-turbine wind farms: Recommendations based on large-eddy simulation. *Sustainable Energy Technol. Assess.* **33**, 34–43 (2019).
38. P. Fleming et al., Initial results from a field campaign of wake steering applied at a commercial wind farm: Part 1. *Wind Energy Sci.* **4**, 273–285 (2019).
39. P. Fleming et al., Field test of wake steering at an offshore wind farm. *Wind Energy Sci.* **2**, 229–239 (2017).
40. J. Annoni et al., "Efficient optimization of large wind farms for real-time control" in *2018 Annual American Control Conference (ACC)* (IEEE, Piscataway, NJ, 2018), pp. 6200–6205.
41. C. R. Shapiro, D. F. Gayme, C. Meneveau, Modelling yawed wind turbine wakes: A lifting line approach. *J. Fluid Mech.* **841**, R1 (2018).
42. M. F. Howland, J. Bossuyt, L. A. Martínez-Tossas, J. Meyers, C. Meneveau, Wake structure in actuator disk models of wind turbines in yaw under uniform inflow conditions. *J. Renewable Sustainable Energy* **8**, 043301 (2016).
43. M. F. Howland, A. S. Ghate, S. K. Lele, Influence of the horizontal component of Earth's rotation on wind turbine wakes. *J. Phys. Conf. Ser.* **1037**, 072003 (2018).
44. P. Gebraad et al., Wind plant power optimization through yaw control using a parametric model for wake effects—a CFD simulation study. *Wind Energy* **19**, 95–114 (2016).
45. D. P. Kingma, J. Ba, Adam: A method for stochastic optimization. arXiv:1412.6980 (30 January 2017).
46. A. Niayifar, F. Porté-Agel, Analytical modeling of wind farms: A new approach for power prediction. *Energies* **9**, 741 (2016).
47. R. J. Stevens, D. F. Gayme, C. Meneveau, Coupled wake boundary layer model of wind-farms. *J. Renewable Sustainable Energy* **7**, 023115 (2015).
48. T. J. Larsen, H. A. Madsen, G. C. Larsen, K. S. Hansen, Validation of the dynamic wake meander model for loads and power production in the Egmond aan Zee wind farm. *Wind Energy* **16**, 605–624 (2013).
49. R. Damiani et al., Assessment of wind turbine component loads under yaw-offset conditions. *Wind Energy Sci.* **3**, 173–189 (2018).
50. D. Medici, "Experimental studies of wind turbine wakes: Power optimisation and meandering," PhD thesis, (KTH Royal Institute of Technology, Stockholm, Sweden) (2005).
51. P. Fleming et al., Simulation comparison of wake mitigation control strategies for a two-turbine case. *Wind Energy* **18**, 2135–2143 (2015).
52. W. Miao, C. Li, J. Yang, X. Xie, Numerical investigation of the yawed wake and its effects on the downstream wind turbine. *J. Renewable Sustainable Energy* **8**, 033303 (2016).
53. F. Campagnolo, V. Petrović, C. L. Bottasso, A. Croce, "Wind tunnel testing of wake control strategies" in *2016 American Control Conference (ACC)* (IEEE, Piscataway, NJ, 2016), pp. 513–518.
54. L. A. Martínez-Tossas, J. Annoni, P. A. Fleming, M. J. Churchfield, The aerodynamics of the curled wake: A simplified model in view of flow control. *Wind Energy Sci.* **4**, 127–138 (2019).
55. P. Fleming et al., Investigation into the shape of a wake of a yawed full-scale turbine. *J. Phys. Conf. Ser.* **1037**, 032010 (2018).
56. K. A. Kragh, M. H. Hansen, Load alleviation of wind turbines by yaw misalignment. *Wind Energy* **17**, 971–982 (2014).
57. J. White, B. Ennis, T. G. Herges, "Estimation of rotor loads due to wake steering" in *2018 Wind Energy Symposium* (AIAA, Reston, VA, 2018), p. 1730.
58. N. Troldborg et al., Numerical simulations of wake interaction between two wind turbines at various inflow conditions. *Wind Energy* **14**, 859–876 (2011).
59. J. Jonkman, *NWTC Design Codes (Fast)* (NREL, Boulder, CO, 2010).